05FTM06

A Model to Predict Friction Losses of Hypoid Gears

by: H. Xu, A. Kahraman, D.R. Houser, The Ohio State University

American Gear Manufacturers Association

TECHNICAL PAPER

A Model to Predict Friction Losses of Hypoid Gears

Hai Xu, Ahmet Kahraman, Donald R. Houser, The Ohio State University

Abstract

A model to predict friction-related mechanical efficiency losses of hypoid gear pairs is proposed, which combines a commercial available finite element based gear contact analysis model and a friction coefficient model with a mechanical efficiency formulation. The contact analysis model is used to provide contact pressures and other contact parameters required by the friction coefficient model. The instantaneous friction coefficient is computed by using a validated new formula that is developed based on a thermal elastohydrodynamic lubrication (EHL) model considering non-Newtonian fluid. Computed friction coefficient distributions are then used to calculate the friction forces and the resultant instantaneous mechanical efficiency losses of the hypoid gear pair at a given mesh angle. The model is applied to study the influence of speed, load, surface roughness, and lubricant temperature as well as assembly errors on the mechanical efficiency of an example face-hobbed hypoid gear pair.

American Gear Manufacturers Association
500 Montgomery Street, Suite 350
Alexandria, Virginia, 22314

October, 2005

ISBN: 1-55589-854-8

A Model to Predict Friction Losses of Hypoid Gears

Hai Xu
Graduate Research Associate

Ahmet Kahraman
Assoc. Professor

Donald R. Houser
Professor Emeritus

Department of Mechanical Engineering
The Ohio State University
650 Ackerman Road, OH 43202

1 Introduction

Gear mesh friction has attracted a number of researchers for more than a century [1]. The friction between gear teeth plays an important role in defining the efficiency of the system as well as influencing scoring limits and the dynamical behavior including vibration and noise [2,3]. Both sliding and rolling actions at the gear mesh contact contribute to gear mesh friction. Sliding friction is a direct product of the relative sliding between the two contacting surfaces while rolling friction originates from the resistance to the rolling motion [4]. Coefficient of friction μ that is used widely in the literature usually refers to the coefficient of sliding friction.

A significant number of studies have been published especially within the last forty years on friction and efficiency of gear trains as reviewed by references [5-7]. The first group of studies focused on measuring power losses of gear pair directly [8-17]. Several others measured μ using twin-disk test machines under conditions simulating a gear pair so that this friction coefficient can be used to predict the efficiency of a gear pair [18-30, 38-39]. Some of these studies [18-25] resulted in well-known and widely used empirical formulae for μ. These empirical formulae indicate that μ is a function of a list of parameters such as sliding and rolling velocities, radii of curvature of the surfaces in contact, load or contact pressure, surface roughness, and the lubricant viscosity.

A group of efficiency models [31-33] investigated the efficiency of a spur gear pair by assuming a uniform μ along the entire contact surface. A tangential friction force along the sliding direction was computed by using a given constant friction coefficient μ, and the geometric and kinematic parameters of the spur gears. As a result, the amount of reduction of torque transmitted to the driven gear was used to calculate the mechanical efficiency η of the gear pair. These models were useful in bringing a qualitative understanding to the role of spur gear geometry on efficiency. They fell short in terms of the definition of μ, as a user-defined constant μ value must be used for every contacting point on the tooth surface. However, the published experiments on sliding/rolling contacts indicate that many parameters might influence μ [18-25]. In addition, these studies were limited to spur gears and many complicating effects of the tooth bending and contact deformations, tooth profile modifications and manufacturing errors were not included.

Another group of efficiency models [34-37, 40] relied on published experimental μ formulae such as those in references [18-21]. The models in this group considered spur [35-37, 40] and helical [34] gear pairs and calculated the parameters required to define μ according to the particular empirical formula adapted. While they are potentially more accurate than the constant μ models, their accuracy is limited to the accuracy of the empirical μ formula used. Each empirical μ formula typically represents a certain type of lubricant, operating temperature, speed and load ranges, and surface roughness conditions of roller specimens that might differ from those of the gear pair that is being modeled.

The models in the last group are more advanced since they use an EHL model to predict μ instead of relying on the user or the empirical formulae [42-54]. Among them, Dowson and Higginson [47], and Martin [48] used a smooth surface EHL model to determine the surface shear stress distribution caused by the fluid film, and hence, the instantaneous friction coefficient at the contact. Adkins and Radzimovsky [49] developed a model for lightly loaded spur gears under hydrodynamic lubrication condition and assumed that the gear tooth is rigid without deflections and local deformations. Simon [50] provided an enhancement by using point contact EHL model for heavily crowned spur gears with smooth surfaces considering the elastic displacement of the surface due to fluid pressure distributions. Larsson [51] and Wang et al [52] analyzed involute spur gear lubrication by using a transient thermal-EHL model with smooth surfaces. Wu and Cheng [53] developed a friction model based on mixed-EHL contacts and applied it to calculate the frictional power losses of

spur gears. The roughness was modeled such that all the asperities have the same radius of curvature whose heights have a Gaussian distribution. Mihalidis et al [54] included the influence of the asperity contacts as well in calculating μ and hence efficiency. These models [47-54] were successful in eliminating to a certain extent the need for prior knowledge of μ, at the expense of significantly more computational effort. While they were relatively enhanced in EHL aspects of the problem, the applications were limited to simple spur gears with ideal load distributions and no tooth bending deformations.

A small number of efficiency studies on helical gears were found [34,40,55-58]. Literature on hypoid gear efficiency is even sparser. Buckingham [59] proposed an approximated formula for the power loss of hypoid gears, which is the sum of the losses of a spiral bevel gear and a worm gear. Naruse et al [8,10] conducted several tests on scoring and frictional losses of hypoid gears of Klingelnberg type. Coleman [60] used a simple formula to calculate hypoid gear efficiency with a constant μ or a μ formula with a very limited number of parameters included [61]. Smooth-surface EHL formulations were found applied to hypoid gears by Simon [62] and Jia et al [63].

1.1 *Objectives and Scope*

Efficiency losses in a gearbox are originated from several sources including gear mesh sliding and rolling friction, windage, oil churning, and bearing friction [34]. When gears are loaded, a gear contact under load experiences combined sliding and rolling, both of which result in frictional losses. The amount of sliding frictional loss is directly related to the coefficient of friction, normal tooth load and relative sliding velocity of the surfaces while the rolling friction occurs due to the deformation of the two contacting surfaces. When the contact is lubricated, rolling frictional losses are originated from the formation of the EHL film [35]. Efficiency can be improved by reducing the coefficient of friction via precision manufacturing and smoothening the contact surfaces and enhancement of lubricant properties. Existing approaches of improving efficiency are based mostly on experimental trial-and-error type procedures focusing on such parameters, while the predictive capabilities have been limited.

The main objective of this study is to develop a mechanical efficiency model for hypoid gears. The model allows an analysis of both face-hobbed and face-milled hypoid gears. The efficiency model will allow two methods of calculating μ, i.e. published empirical formulae and a thermal EHL formulation. The differences amongst these approaches will be described. Parametric studies will be performed to investigate the influence of several relevant parameters such as speed, load, surface roughness, lubricant temperature as well as the assembly errors on the mechanical efficiency of hypoid gears. This study is focused primarily on the mechanical efficiency losses related to tooth friction, including sliding and rolling friction, while it relies on the published studies in terms of losses associated with windage, oil churning and bearings [34,35,64-69] when necessary.

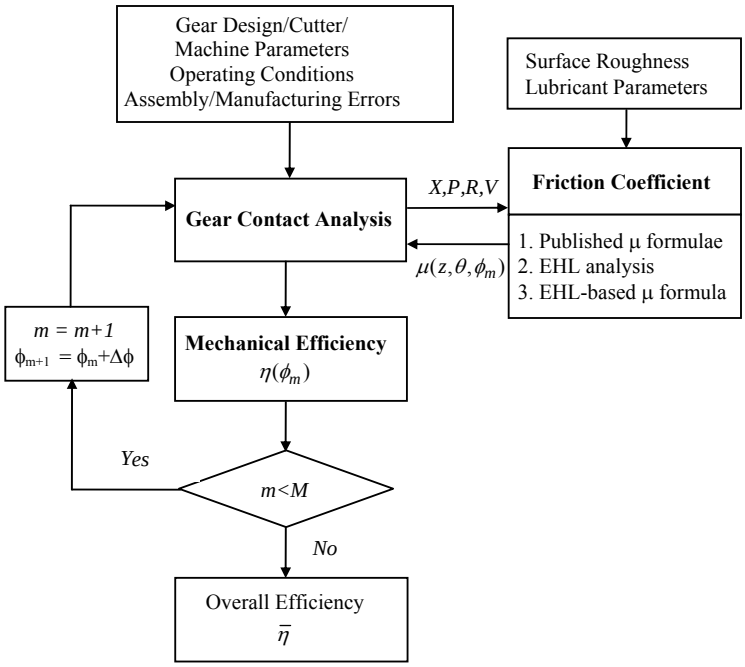

Figure 1. Flowchart for the efficiency prediction.

2 Efficiency Model

2.1 *Technical Approach*

Figure 1 illustrates a flowchart of the efficiency computation methodology used in this study. Three main components are the gear contact analysis model, the friction coefficient computation model, and the gear pair mechanical efficiency computation formulation. The same methodology was applied by these authors earlier to spur and helical gears successfully [70]. It was also shown the parallel-axis efficiency model compares well with the gear pair efficiency experiments [77]. The gear contact analysis model uses the gear design parameters, operating conditions and errors associated with assembly, mounting and manufacturing of the tooth profile to predict load and contact pressure distributions at every contact point during each mesh position. Predicted load distribution or contact

pressure together with other geometric and kinematic parameters are input to the friction coefficient model to determine the instantaneous friction coefficient $\mu(z,\theta,\phi_m)$ of every contact point (z,θ) on the gear tooth surface. $\mu(z,\theta,\phi_m)$ is then used by the mechanical efficiency computation module to determine the instantaneous efficiency $\eta(\phi_m)$ of the gear pair at the *m*-th incremental rotational position defined by angle ϕ_m. The above sequential procedure is repeated for an *M* number of discrete positions ($m = 1,2,\ldots,M$) spaced at an increment of $\Delta\phi$ ($\phi_m = m\,\Delta\phi$) to cover an entire mesh cycle. These instantaneous mechanical efficiency values $\eta(\phi_m)$ are then averaged over a complete mesh cycle to obtain the average mechanical efficiency loss of the gear pair due to tooth friction. In the following sections, main components of this methodology as shown in Fig. 1 are described in detail.

2.2 *Contact Analysis of Hypoid Gears*

A commercial available finite element (FE) based hypoid gear analysis package CALYX [71] is used as the contact analysis tool. Both face-hobbed and face-milled versions of this model are available. The model combines FE method away from the contact zone with a surface integral formulation applied at and near the contact zone [72]. The contact analysis model used in this study has a special setup for the finite element grids inside the instantaneous contact zone. As shown in Fig. 2(a), a set of very fine contact grid is defined automatically on hypoid gear teeth to capture the entire contact zone. These grid cells are much finer than the regular size of finite element meshes elsewhere on the tooth surfaces and they are attached to the contact zones that result in more accurate contact analysis. A schematic view of these grid cells is shown in Fig. 2(b). Along the face width, there are 2*n*+1 divisions, and at each division, there is a principal contact point (shown in dot) if contact occurs. In the profile direction, there are 2*m*+1 grid cells within each division for capturing potential contact points, which would be in contact due to tooth deflections and local surface deformations.

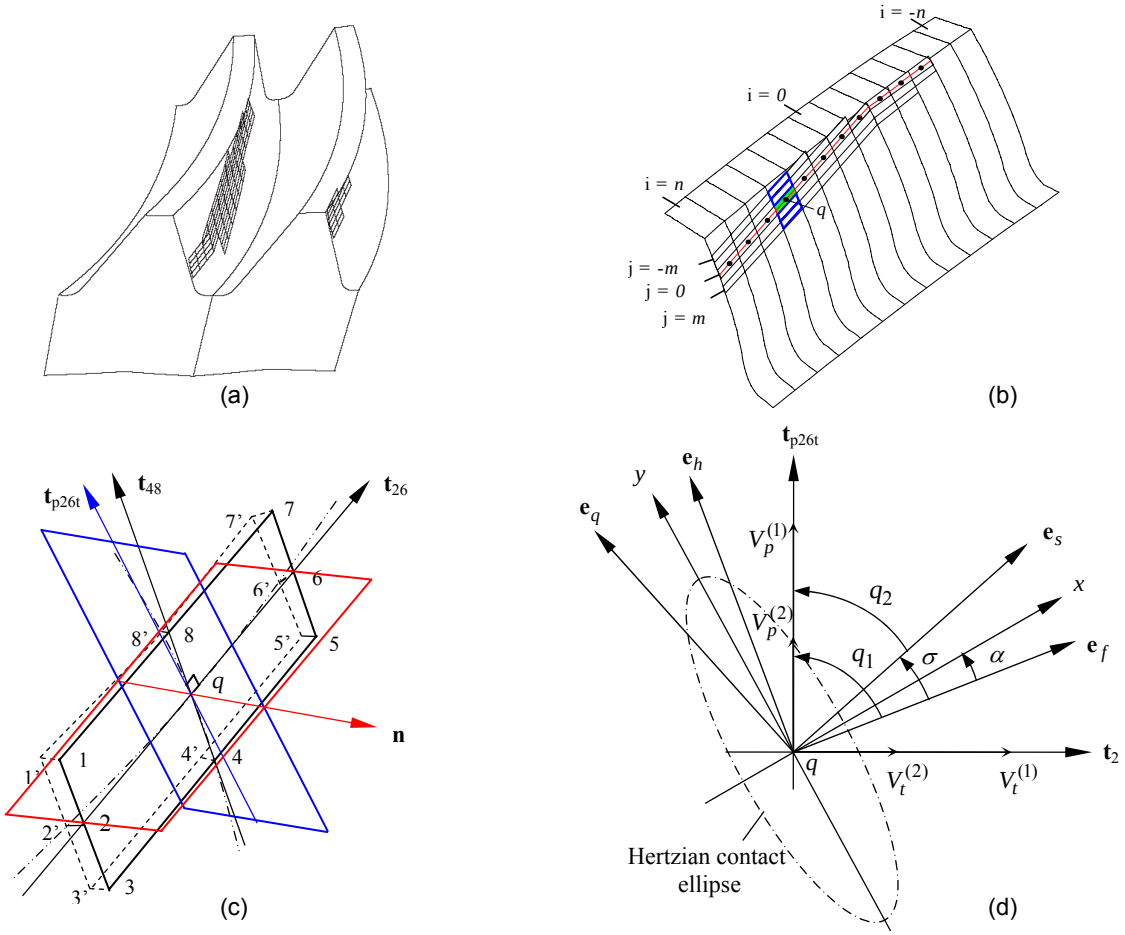

Figure 2. (a) Moving grids for contact zones, (b) moving grid setup, (c) grid in tangent plane for μ calculation, and (d) principal directions and contact ellipse.

The μ calculation is carried out in the grid of principal contact point in the tangent plane as shown in Fig. 2(c), which is a magnified grid cell for the principal contact point q. The surface formed by dotted lines, with points 1' to 8' along the edges, is the grid on the real tooth surface and the plane formed by solid lines, with points 1 to 8 along the edges, is the grid in the tangent plane for this particular contact point q. Points 2(2'), 4(4'), 6(6') and 8(8') are the mid point at each side of the grids. Vector $\mathbf{t}_{26}$ that connects point 2 and 6 is approximated as the instant line of contact and vector $\mathbf{t}_{p26t}$ is normal to $\mathbf{t}_{26}$ in the tangent plane. $\mathbf{n}$ is the surface normal vector at the contact point q. When μ is obtained for this principal contact point, same μ value will be assigned to the potential contact point within the same face width division. While the load distribution and contact pressure at each grid is provided by the contact analysis model, surface velocities and curvatures are calculated in the following sections.

Definition of Principal Contact Points. Assume pinion surface and gear surface are defined by $\mathbf{r}_1(s_1,t_1)$ and $\mathbf{r}_2(s_2,t_2)$ respectively, where s_1, t_1 and s_2, t_2 are the surface curvilinear parameters. The principal contact point is determined and located when $\mathbf{r}_1$ and $\mathbf{r}_2$ become the closest to each other [72]. Surface $\mathbf{r}_1(s_1,t_1)$ was discretized into a grid of points $\mathbf{r}_{1ij}=\mathbf{r}_1(s_{1i},t_{1j})$ and for each of these grid points, an effort was made to locate $\mathbf{r}_{2ij}=\mathbf{r}_2(s_{2i},t_{2j})$ such that $\left\|\mathbf{r}_1(s_1,t_1)-\mathbf{r}_2(s_2,t_2)\right\|$ is minimized with respect to the variable s_2 and t_2. This extremization is equivalent to solving the following system of nonlinear equations [72]

$$\begin{cases} \left[\mathbf{r}_{1ij}-\mathbf{r}_2(s_{2i},t_{2j})\right]\partial\mathbf{r}_2(s_{2i},t_{2j})/\partial s_{2i}=0 \\ \left[\mathbf{r}_{1ij}-\mathbf{r}_2(s_{2i},t_{2j})\right]\partial\mathbf{r}_2(s_{2i},t_{2j})/\partial s_{2j}=0 \end{cases} \tag{1}$$

First, solutions from Eq. (1) for each of the grid point $\mathbf{r}_{1ij}$ were obtained by the Newton-Raphson method. Then a new grid, which is finer than the original grid, was set up around the point $\mathbf{r}_{1ij}$ for which the separation $\left\|\mathbf{r}_{1ij}-\mathbf{r}_{2ij}\right\|$ was the smallest. This search process is repeated several times with progressively smaller grids to locate the principal contact point [72]. The pinion and gear surfaces were divided in several parts along the face width. In each face width division, if there is contact, the principal contact is determined and then a set of grids is laid out above and below the principal contact point. These grids are added for candidate contact points that will likely be in contact due to elastic deformations of the two contacting surfaces.

Calculation of Principal Curvatures and Principal Directions. According to differential geometry [73], for two surfaces in contact at a common point, the principal curvatures and principal directions at the common point can be determined if the coefficients of the first and second fundamental form of the surface are given. Let $\kappa^{(1)}$ and $\kappa^{(2)}$ be the two eigenvalues of the eigen problem

$$\mathbf{N}\boldsymbol{\lambda}=\kappa\mathbf{M}\boldsymbol{\lambda} \tag{2}$$

where

$$\boldsymbol{\lambda}=\begin{Bmatrix}\lambda_1\\ \lambda_2\end{Bmatrix},\qquad \mathbf{M}=\begin{bmatrix}\frac{\partial\mathbf{r}}{\partial s}\cdot\frac{\partial\mathbf{r}}{\partial s} & \frac{\partial\mathbf{r}}{\partial s}\cdot\frac{\partial\mathbf{r}}{\partial t}\\ \frac{\partial\mathbf{r}}{\partial t}\cdot\frac{\partial\mathbf{r}}{\partial s} & \frac{\partial\mathbf{r}}{\partial t}\cdot\frac{\partial\mathbf{r}}{\partial t}\end{bmatrix},$$

$$\mathbf{N}=\begin{bmatrix}\mathbf{n}\cdot\frac{\partial^2\mathbf{r}}{\partial s^2} & \mathbf{n}\cdot\frac{\partial^2\mathbf{r}}{\partial s\partial t}\\ \mathbf{n}\cdot\frac{\partial^2\mathbf{r}}{\partial t\partial s} & \mathbf{n}\cdot\frac{\partial^2\mathbf{r}}{\partial t^2}\end{bmatrix},\qquad \mathbf{n}=\frac{\frac{\partial\mathbf{r}}{\partial s}\times\frac{\partial\mathbf{r}}{\partial t}}{\left\|\frac{\partial\mathbf{r}}{\partial s}\times\frac{\partial\mathbf{r}}{\partial t}\right\|}.$$

Here, $\mathbf{n}$ is the unit normal vector, and s and t are the surface curvilinear parameters at the common contact point. Matrices $\mathbf{M}$ and $\mathbf{N}$ contain the coefficients of the first and second fundamental form of the surface, respectively. Then $\kappa^{(1)}$ and $\kappa^{(2)}$ are the principal normal curvatures. If the two corresponding eigenvectors $\boldsymbol{\lambda}^{(1)}$ and $\boldsymbol{\lambda}^{(2)}$ are normalized such that $\{\boldsymbol{\lambda}^{(i)}\}^{\mathrm{T}}\mathbf{M}\boldsymbol{\lambda}^{(i)}=1$, $i=1,2$, then the two unit vectors in the principal directions corresponding to the principal curvatures are defined as [72]

$$\mathbf{e}^{(1)}=\{\boldsymbol{\lambda}^{(1)}\}^{\mathrm{T}}\begin{Bmatrix}\partial\mathbf{r}/\partial s\\ \partial\mathbf{r}/\partial t\end{Bmatrix}, \tag{3a}$$

$$\mathbf{e}^{(2)}=\{\boldsymbol{\lambda}^{(2)}\}^{\mathrm{T}}\begin{Bmatrix}\partial\mathbf{r}/\partial s\\ \partial\mathbf{r}/\partial t\end{Bmatrix}. \tag{3b}$$

Determination of The Orientation of the Contact Ellipse. Assume q is the contact point of surface Σ_1 and surface Σ_2. Let $\mathbf{e}_f$ and $\mathbf{e}_h$ be unit vectors of principal directions, and κ_f and κ_h be principal curvatures of surface Σ_1 at point q. Let $\mathbf{e}_s$ and $\mathbf{e}_q$ be unit vectors of principal directions, and κ_s and κ_q be principal curvatures of surface Σ_2 at point q. These values of principal directions and curvatures can be solved by Eq. (2). The angle σ, formed by $\mathbf{e}_f$ and $\mathbf{e}_s$, and the angle α that determines the orientation of the coordinate axes x and y with respect to $\mathbf{e}_f$ as shown in Fig. 2(d) can be obtained as [72]

$$\sigma = \tan^{-1}\left(\frac{\mathbf{e}_s \cdot \mathbf{e}_h}{\mathbf{e}_s \cdot \mathbf{e}_f}\right), \tag{4a}$$

$$\alpha = \frac{1}{2}\tan^{-1}\left(\frac{g_2 \sin 2\sigma}{g_1 - g_2 \cos 2\sigma}\right) \tag{4b}$$

where $g_1 = \kappa_f - \kappa_h$, and $g_2 = \kappa_s - \kappa_q$. Then the two directions x and y can be represented as

$$x = \mathbf{e}_f \cos\alpha + \mathbf{e}_h \sin\alpha, \tag{5a}$$

$$y = -\mathbf{e}_f \sin\alpha + \mathbf{e}_h \cos\alpha. \tag{5b}$$

Calculation of Surface Velocities and Radii of Curvatures in the Desired Directions. Consider that two bodies are in point contact or line contact in space and the two contacting surfaces, Σ_1 and Σ_2, are in continuous tangency at the point of contact. The position vectors and unit normals of surface Σ_1 and surface Σ_2 must be equal. Based on this consideration, the following two relations can be obtained [74]

$$\mathbf{v}_r^{(2)} = \mathbf{v}_r^{(1)} + \mathbf{v}^{(12)} \tag{6a}$$

$$\dot{\mathbf{n}}_r^{(2)} = \dot{\mathbf{n}}_r^{(1)} + \boldsymbol{\omega}^{(12)} \times \mathbf{n} \tag{6b}$$

where $\mathbf{v}_r^{(i)}$ is the relative velocity vector of the contact point respect to the surface as it moves over the surface Σ_i, $\dot{\mathbf{n}}_r^{(i)}$ is the velocity of the tip of the surface unit normal in its motion over the surface Σ_i, $\mathbf{n}$ is the surface unit normal vector, and $\boldsymbol{\omega}^{(12)} = \boldsymbol{\omega}^{(1)} - \boldsymbol{\omega}^{(2)}$. Equations (6a,b) are then used for the derivation of curvature relations of mating surfaces. As shown in Fig. 2(d), velocity vectors of point q on surface Σ_1 can be represented in coordinate system $S_a(\mathbf{e}_f, \mathbf{e}_h)$ as

$$\mathbf{v}_r^{(1)} = \begin{bmatrix} v_f^{(1)} & v_h^{(1)} \end{bmatrix}^T, \tag{7a}$$

$$\dot{\mathbf{n}}_r^{(1)} = \begin{bmatrix} \dot{n}_f^{(1)} & \dot{n}_h^{(1)} \end{bmatrix}^T. \tag{7b}$$

Velocity vectors of point q on surface Σ_2 can be represented in coordinate system $S_b(\mathbf{e}_s, \mathbf{e}_q)$ as

$$\mathbf{v}_r^{(2)} = \begin{bmatrix} v_s^{(2)} & v_q^{(2)} \end{bmatrix}^T, \tag{8a}$$

$$\dot{\mathbf{n}}_r^{(2)} = \begin{bmatrix} \dot{n}_s^{(2)} & \dot{n}_q^{(2)} \end{bmatrix}^T. \tag{8b}$$

According to Rodrigues' formula, vectors $\mathbf{v}_r^{(i)}$ and $\dot{\mathbf{n}}_r^{(i)}$ are collinear for the principal directions, and they are related to the principal directions as $\dot{\mathbf{n}}_r^{(i)} = -\kappa_{I,II}^{(i)} \mathbf{v}_r^{(i)}$ [74], where $\kappa_{I,II}^{(i)}$ are the principal curvatures of surface Σ_i, $i = 1, 2$. These principal surface are κ_f and κ_h for surface Σ_1 and κ_s and κ_q for surface Σ_2. With the aid of Rodrigues' formula, Eqs. (7,8) are rearranged together with appropriate coordinate transformations to get a system of linear equations as [74]

$$\begin{bmatrix} b_{11} & b_{12} & 0 & 0 \\ b_{21} & b_{22} & 0 & 0 \\ 0 & 0 & b_{33} & b_{34} \\ 0 & 0 & b_{43} & b_{44} \end{bmatrix} \begin{Bmatrix} v_h^{(2)} \\ v_f^{(2)} \\ v_s^{(1)} \\ v_q^{(1)} \end{Bmatrix} = \begin{bmatrix} b_{15} \\ b_{25} \\ b_{35} \\ b_{45} \end{bmatrix} \tag{9}$$

where

$$\begin{aligned}
b_{11} &= -\kappa_f + \kappa_s \cos^2\sigma + \kappa_q \sin^2\sigma, \\
b_{12} &= b_{21} = \kappa_s \sin\sigma\cos\sigma - \kappa_q \sin\sigma\cos\sigma, \\
b_{22} &= -\kappa_h + \kappa_s \sin^2\sigma + \kappa_q \cos^2\sigma, \\
b_{33} &= \kappa_s - \kappa_f \cos^2\sigma - \kappa_h \sin^2\sigma, \\
b_{34} &= b_{43} = \kappa_f \sin\sigma\cos\sigma - \kappa_h \sin\sigma\cos\sigma, \\
b_{44} &= \kappa_q - \kappa_f \sin^2\sigma - \kappa_h \cos^2\sigma, \\
b_{15} &= -(\boldsymbol{\omega}^{(12)} \cdot \mathbf{e}_h) - \kappa_f (\mathbf{v}^{(12)} \cdot \mathbf{e}_f), \\
b_{25} &= (\boldsymbol{\omega}^{(12)} \cdot \mathbf{e}_f) - \kappa_h (\mathbf{v}^{(12)} \cdot \mathbf{e}_h), \\
b_{35} &= -(\boldsymbol{\omega}^{(12)} \cdot \mathbf{e}_q) - \kappa_s (\mathbf{v}^{(12)} \cdot \mathbf{e}_s), \\
b_{45} &= (\boldsymbol{\omega}^{(12)} \cdot \mathbf{e}_s) - \kappa_q (\mathbf{v}^{(12)} \cdot \mathbf{e}_q).
\end{aligned}$$

Equation (9) can then be solved to obtain the surface velocities in the principal directions. The surface velocities in the direction of contact line and in the direction that is normal to the contact line for surface Σ_1 and surface Σ_2, as shown in Fig. 2(d), can then be obtained by coordinate transformation as follows

$$\begin{bmatrix} V_p^{(1)} \\ V_t^{(1)} \end{bmatrix} = \begin{bmatrix} \cos q_2 & \sin q_2 \\ -\sin q_2 & \cos q_2 \end{bmatrix} \begin{bmatrix} v_s^{(1)} \\ v_q^{(1)} \end{bmatrix} \tag{10a}$$

$$\begin{bmatrix} V_p^{(2)} \\ V_t^{(2)} \end{bmatrix} = \begin{bmatrix} \cos q_1 & \sin q_1 \\ -\sin q_1 & \cos q_1 \end{bmatrix} \begin{bmatrix} v_f^{(2)} \\ v_h^{(2)} \end{bmatrix} \tag{10b}$$

Then, sliding and rolling velocities in the direction of the contact line can be obtained as $V_{st} = V_t^{(1)} - V_t^{(2)}$ and $V_{rt} = V_t^{(1)} + V_t^{(2)}$, respectively. Sliding and rolling velocities in the direction that is normal to the contact line are $V_{sp} = V_p^{(1)} - V_p^{(2)}$ and $V_{rp} = V_p^{(1)} + V_p^{(2)}$, respectively. The resultant sliding and rolling velocities are given as $V_{stotal} = (V_{st}^2 + V_{sp}^2)^{0.5}$ and $V_{rtotal} = (V_{rt}^2 + V_{rp}^2)^{0.5}$, respectively. Normal curvatures in the direction of the contact line, $\kappa_{nc}^{(i)}$, and in the direction that is normal to the contact line, $\kappa_{nn}^{(i)}$, can be obtained as follows

$$\kappa_{nc}^{(i)} = \kappa_I^{(i)} \cos^2(\pi/2 + q_i) + \kappa_{II}^{(i)} \sin^2(\pi/2 + q_i) \tag{11a}$$

$$\kappa_{nn}^{(i)} = \kappa_I^{(i)} \cos^2 q_i + \kappa_{II}^{(i)} \sin^2 q_i \tag{11b}$$

Table 1 Empirical friction coefficient formulae considered in this study (ν_k and ν are given in centistokes and centipoises, respectively).

Formula and author	Applicable parameter ranges	Specific units
Drozdov and Gavrikov [21]: $\mu = [0.8\sqrt{\nu_k} V_s + V_r\phi + 13.4]^{-1}$ $\phi = 0.47 - 0.13\,(10)^{-4} P_{\max} - 0.4(10)^{-3}\nu_k$	$\nu_k \in [4,500]$ $V_s \le 15$, $V_r \in [3,20]$ $P_{\max} \in [4000, 20000]$	V_s, V_r = m/s $P_{\max}$ = kg/cm^2
O'donoghue and Cameron [20] $\mu = 0.6\left[(S+22)/35\right]\left[\nu^{1/8} V_s^{1/3} V_r^{1/6} R^{1/2}\right]^{-1}$		S = μin , CLA V_s, V_r = in/s , R = in
Misharin [18] $\mu = 0.325\left[V_s V_r \nu_k\right]^{-0.25}$	$V_s / V_r \in [0.4, 1.3]$ $P \ge 2{,}500$, $\mu \in [0.02, 0.08]$	V_s, V_r = m/s P = kg/cm^2
ISO TC60 [41] $\mu = 0.12\left[W' S/(R V_r \nu)\right]^{0.25}$		V_r = m/s , R = mm S = μm , RMS, W' = N/mm
Benedict and Kelley [19] $\mu = 0.0127\left[\frac{50}{50-S}\right] Log_{10}\left[\frac{3.17(10)^8 W'}{\nu V_s V_r^2}\right]$	$\frac{50}{50-S} \le 3$	S = μin , RMS W' = lbf/in V_s, V_r = in/s

where, q_i is the angle that is formed by the direction of interest and $\mathbf{e}_f$ and $\mathbf{e}_s$ for $i=1$ and $i=2$, respectively. Then the radius of curvature is simply the inverse of the corresponding normal curvature value in Eq. (11).

2.3 *Friction Coefficient Models*

Empirical Friction Coefficient Formulae. A large number of empirical formulae for coefficient of friction can be found in the literature. Most of these formulae obtained from measured data of twin-disk type tests were in the following general form

$$\mu = f\left(\nu_k, \nu, V_s, V_r, R, W', P_{\max}, S, \ldots\right). \qquad (12)$$

Here ν_k and ν are kinematic and dynamic viscosity of the lubricant, both of which are measured at the oil inlet, and are function of inlet oil temperature at ambient pressure. Parameters V_s, V_r, and R denote relative surface sliding velocity, sum of the rolling velocities and the combined radius of curvature, respectively. The load parameters are the unit normal load W' or the contact pressure $P_{\max}$. S is a surface finish parameter, representing the initial composite surface roughness of the two contacting surfaces.

A representative set of commonly cited μ formulae given in Table 1 are considered in this study. These formulae are quite different from each other as they consider different parameters and parameter ranges. Formulae by Drozdov and Gavrikov [21] and Misharin [18] include neither any surface roughness parameter nor a radius of curvature R, while others consider a surface roughness parameter S (root-mean-square (RMS) or centerline average (CLA)). ISO TC60 [41] formula does not include V_s while formulae of O'donoghue and Cameron [20] and Misharin [18] do not consider the load as a parameter and hence they should not be able to account for any load effects on μ. In addition, each formula listed in Table 1 is valid for a range of key system parameters. For instance, the formula proposed by Drozdov and Gavrikov is valid for $\nu_k \in [4,500]$ centistokes, $V_s \le 15$ m/s, $V_r \in [3,20]$ m/s and $P_{\max} \in [4000, 20000]$ kg/cm^2, and would be suitable for a gear application only if these gear contact parameters stay within these ranges.

Calculation of Friction Coefficient Using an EHL Model. According to EHL theory, distribution of the film pressure and thickness across an elastic lubricated contact can be obtained by solving the transient Reynolds equation simultaneously with a number of other equations including the film thickness equation, the energy balance equation, viscosity-pressure-temperature relationship, density-pressure-temperature relationship, and the load equation [75]. In this study, a deterministic EHL model based on the model proposed by Cioc et al [75] will be used. Assuming that a hypoid gear pair exhibits line contact conditions, a non-dimensional transient Reynolds equation is written as

$$\frac{\partial}{\partial X}\left[s\left(\frac{P_h b}{12\nu_0 u}\right)\left(\frac{\bar{\rho} H^3}{\bar{\nu}}\right)\frac{\partial P}{\partial X}\right] = \frac{\partial}{\partial X}\left(\bar{\rho} H\right) + \frac{\partial}{\partial \bar{t}}\left(\bar{\rho} H\right) \qquad (13)$$

with the boundary conditions of $P=0$ at inlet, and $P=0$ and $\partial P/\partial X=0$ at outlet. In Eq. (13), b is the half width of Hertzian contact zone, and X and H are the dimensionless coordinate and the dimensionless film thickness, respectively, both normalized by b, P_h is the maximum Hertzian pressure, $\bar{\nu}$ is the dimensionless dynamic viscosity normalized by ν_0, which is the dynamic viscosity at oil inlet, and $\bar{\rho}$ is the dimensionless lubricant density normalized by the lubricant density at inlet. u is the rolling velocity defined as $u=(u_1+u_2)/2$ and $\bar{t}$ is the dimensionless time defined as $\bar{t}=ut/b$. For a Newtonian fluid $s=1$ while s is defined by a nonlinear function for a non-Newtonian fluid [75]. The film thickness equation has the form

$$H=\frac{h_0}{b}+(\frac{b}{2R})X^2+\frac{d(X,\bar{t})}{b}+S\left(X,\bar{t}\right) \tag{14}$$

where, h_0 is the reference film thickness, $d(X,\bar{t})$ is the total elastic deformation, $S\left(X,\bar{t}\right)$ is the composite surface profile irregularities, and R is the combined radius of curvature of the contact. A two-slope viscosity-pressure-temperature model [75] is used here as

$$\nu=\begin{cases} e^{[G_1P-\bar{\gamma}(T-1)]}, & P<P_a, \\ e^{[c_0+c_1P+c_2P^2+c_3P^3-\bar{\gamma}(T-1)]}, & P_a\le P\le P_b, \\ e^{[G_1P_t+G_2(P-P_t)-\bar{\gamma}(T-1)]}, & P_b\le P. \end{cases} \tag{15}$$

Here, $G_1=\alpha_1P_h$, $G_2=\alpha_2P_h$, $\bar{\gamma}$ is the dimensionless coefficient of thermal expansion, and T is the dimensionless film temperature normalized by the oil temperature at inlet. P_t is the transitional pressure, a threshold value beyond which an increase in viscosity changes its slope from α_1 to α_2. Transition pressure values of $P_a=0.7P_t$ and $P_b=1.4P_t$ are used with $P_t=380$ *MPa* as suggested by Allen for mineral oils [75]. The coefficients c_0 to c_3 are determined such that that transition between the two slopes is smooth. In addition, the following density-pressure-temperature relationship is considered

$$\bar{\rho}=\left(1+\frac{C_aP}{1+C_bP}\right)\left[1-\bar{\beta}\left(T-1\right)\right] \tag{16}$$

where $C_a=0.6\times10^{-9}P_h$, $C_b=1.7\times10^{-9}P_h$, and $\bar{\beta}$ is the dimensionless coefficient of thermal expansion [75].

Since a thermal EHL model is sought, the energy equation for non-Newtonian lubricants is given as

$$\frac{\partial^2T}{\partial Z^2}=C_1U\bar{\rho}\frac{\partial T}{\partial X}-C_2TU\frac{\partial P}{\partial X}-C_3\frac{\bar{\tau}_1\bar{\tau}_L}{\bar{\nu}\sqrt{(\bar{\tau}_L)^2-(\bar{\tau}_1)^2}}+C_4\bar{\rho}\frac{\partial T}{\partial\bar{t}} \tag{17}$$

In Eq. (17), coefficients C_i ($i=1$ to 4) are functions of thermal parameters, Z is the dimensionless coordinate normalized by b, U is the dimensionless fluid velocity, $\bar{\tau}_1$ is the dimensionless shear stress of surface 1, and $\bar{\tau}_L$ is the dimensionless limiting shear stress. Finally, the load distribution predicted should be such that the normal load applied at the contact is balanced, i.e.

$$\bar{W}=\int_{X_{in}}^{X_{out}}\left[P(X,\bar{t})+P_c(X,\bar{t})\right]dX \tag{18}$$

where $\bar{W}$ is the dimensionless unit load applied, X_{in} and X_{out} are the inlet and outlet of computational domain for the contact zone, P_c is the asperity contact pressure for where asperity contact occurs. This load balance equation is checked periodically and the reference film thickness h_0 in Eq. (14) is adjusted, if necessary.

In reference [75], Eqs. (13-18) were solved numerically by using the finite difference method. Using the same methodology, distributions of the pressure $p(x)$, viscosity $\nu(x)$, and fluid film thickness $h(x)$ across the lubricated contact zone are predicted. In the case of no asperity contacts, the surface shear stress distribution across the Hertzian contact width $-b\le x\le b$ is given by

$$\tau(x)=-\frac{h(x)}{2}\frac{\partial p}{\partial x}+\nu(x)\frac{u_1-u_2}{h(x)}. \tag{19}$$

Typical ground or shaved gear tooth surfaces cannot be considered smooth unless they are polished chemically or mechanically. The actual surface roughness amplitudes are typically comparable to the fluid film thickness. As a result, the portion of the normal load might be carried by actual asperity contacts resulting in mixed- or partial-EHL conditions. In this case, Eq. (19) is still valid at the *x* locations where a fluid film is maintained between the two surfaces. At the *x* locations where actual asperity contacts take place

$$\tau(x)=\mu_sp(x) \tag{20}$$

where μ_s is the friction coefficient between the contacting asperities. Consequently, the friction traction force per unit width of the contact can be written as

$$F_t = \int \tau(x)dx = F_r' + F_s' \tag{21}$$

where F_r' is the rolling friction per unit width of the contact that comes from the viscous flow in the formation of the film thickness and squeeze motion during pure rolling,

$$F_r' = -\int \frac{h(x)}{2}\frac{\partial p}{\partial x}dx \tag{22}$$

and F_s' is the sliding friction per unit width of the contact that is caused by fluid shear and the asperity contact, respectively [76]

$$F_s' = \int \nu(x)\frac{u_1 - u_2}{h(x)}dx + \int \mu_s p(x)dx\ . \tag{23}$$

Finally, the coefficient of sliding friction of the entire section of contact is given by $\mu = F_s'/W'$ where W' is the applied normal load per unit width of contact.

With the exception of μ_s in Eq. (23) that must be defined in cases when asperity contact occurs, the approach outlined above to compute μ is entirely physics-based. One disadvantage of this approach is that it requires significant computational effort since a large number of individual EHL analysis must be carried out for each discretized segment along the lines of contact at each rotational gear position considered.

2.4 *Gear Efficiency Computation*

Once the coefficient of friction $\mu(z,\theta,\phi_m)$ at each contact point (z,θ) at each rotational angle ϕ_m ($m = 1,2,\ldots,M$) are known, the sliding friction force at each contact position can be calculated by

$$F_s(z,\theta,\phi_m) = \mu(z,\theta,\phi_m)W(z,\theta,\phi_m) \tag{24}$$

where $W(z,\theta,\phi_m)$ is the normal load at the contact point of interest. The rolling friction force F_r can be obtained by multiplying F_r' in Eq. (22) with the width of the contact. When the empirical formulae like the ones listed in Table 1 are used, F_r can be estimated from an isothermal EHL contact [53] as

$$F_{ro} = 4.318(\tilde{G}\tilde{U})^{0.658}\tilde{Q}^{0.0126}R/\alpha \tag{25}$$

where $\tilde{G} = \alpha E'$ is the dimensionless material parameter, $\tilde{U} = \nu_0(u_1 + u_2)/(E'R)$ is the dimensionless speed parameter, $\tilde{Q} = W'/(E'R)$ is the dimensionless load parameter, R is the effective radius of curvature, α is the pressure viscosity coefficient. In order to account for the effect of temperature rise at high speed conditions, a thermal reduction factor φ_T can be used to modify this isothermal formula such that

$$F_r = \varphi_T F_{ro} \tag{26}$$

where φ_T is defined in reference [53] as

$$\varphi_T = \frac{1 - 13.2(P_h/E')(L^*)^{0.42}}{1 + 0.213(1 + 2.23SR^{0.83})(L^*)^{0.64}}\ , \tag{27}$$

$$L^* = -\frac{\partial \nu}{\partial t_0}\frac{(V_e)^2}{K_f}\ . \tag{28}$$

Here, ν is the absolute viscosity in cPs, t_0 is the lubricant temperature at inlet in degrees C, K_f is the lubricant thermal conductivity in $W/m^\circ C$, SR is the slide-to-roll ratio that is defined as $SR = 2(u_1 - u_2)/(u_1 + u_2)$, and $V_e = (u_1 + u_2)/2$.

The instantaneous efficiency of a gear pair is defined as the ratio of the instantaneous output power to the input power

$$\eta(\phi_m) = \frac{L_{out}(\phi_m)\omega_{out}}{L_{in}\omega_{in}} \tag{29}$$

where $L_{out}(\phi_m)$ and L_{in} are the values of torque acting on the output and input gears and ω_{out} and ω_{in} are the output and input rotational speeds, respectively. When only frictional losses are considered, the instantaneous output power can be written as the difference between the input power and the frictional power losses and hence the efficiency can be expressed as

$$\eta(\phi_m) = 1 - \frac{1}{L_{in}\omega_{in}}\sum_{q=1}^{Q}\left[\left|F_s(u_1 - u_2)\right| + \left|F_r(u_1 + u_2)\right|\right]_q \tag{30}$$

where the summation from $q = 1$ to Q is the sum of sliding frictional and rolling frictional power losses at position ϕ_m and Q is the total number of load grids at the same mesh position.

2.5 *Validation of Friction Coefficient Models*

Comparison of Empirical and the EHL-Based μ Models. In order to facilitate numerical comparisons among these formulae and the EHL model predictions, an example line contact problem with the following parameters is considered:

$$R = 5\ \ mm,\ V_e = 5\ \ m/s,\ P_h = 2\ \ GPa\ ,$$
$$\nu_0 = 10\ \ cPs,\ \nu_k = 13\ \ cSt,\ S_{rms} = 0.07\ \ \mu m\ .$$

With these parameters, the calculated μ values from published empirical formulae in Table 1, and

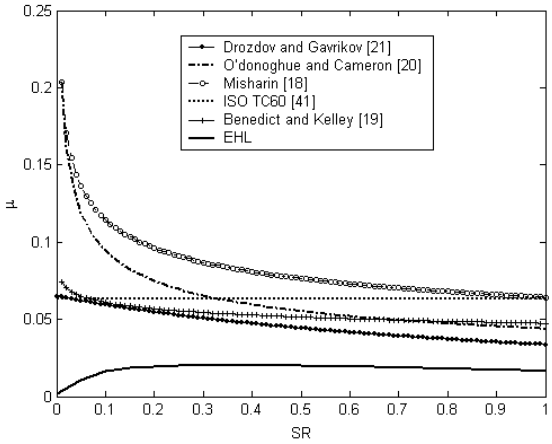

Figure 3. Comparison of friction coefficient models for $R = 5\,mm$, $V_e = 5\,m/s$, $P_h = 2\,GPa$, $\nu_0 = 10$ *cPs*, $\nu_k = 13$ *cSt*, and $S_{rms} = 0.07\,\mu m$.

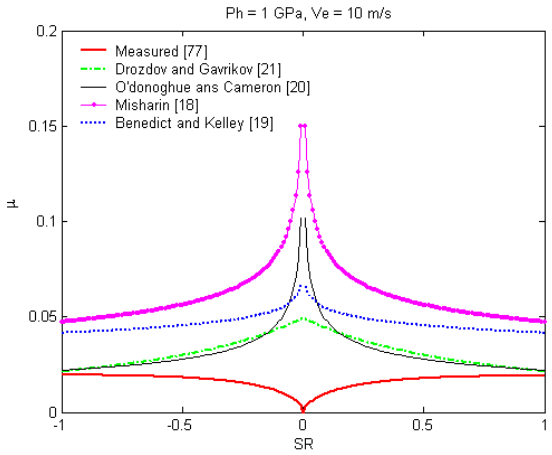

Figure 4. Comparison between published empirical friction coefficient formulae and the measured traction data.

from the thermal EHL model described in section 2.3 are plotted as a function of SR in Fig. 3. Here, three main discrepancies between the published empirical formulae and the thermal EHL-based μ are evident. (i) When $SR = 0$, EHL model predicts nearly zero friction, while published empirical formulae all predict their largest μ values. This is because V_s is in the denominator of most of these formulae. This implies that the friction coefficient is largest at the pitch point where there is no relative sliding in total conflict with the physical intuition and the EHL model prediction. (ii) The overall qualitative shape of the μ versus SR curve from the EHL model is very different from those obtained from the other μ formulae. (iii) The thermal EHL model predicts much lower μ values than the empirical formulae, regardless of the value of SR. Since the differences amongst the individual μ formulae as well as between the EHL model and these formulae are very significant, neither can be used in the efficiency model with confidence since the resultant efficiency predictions will differ greatly. Only way to describe these discrepancies is to compare the predicted coefficients of friction to the measured ones.

A comparison between the published empirical μ formulae and the measured traction data is shown in Fig. 4. The discrepancies between these published formulae and the fitted measured data are quite similar to those between the same formulae and the EHL model predictions in Fig. 3. In Fig. 4, for $V_e = 10$ m/s and $P_h = 1.0$ GPa, the measured and predicted μ values differ in both magnitudes and qualitative shape. The published empirical formulae of others give larger μ values regardless the value of SR. The predicted μ values become very large as SR approaches zero while the measured μ value is almost zero at $SR = 0$. Typical gear pairs might have SR values between –1 and 1. The same differences were observed at other load and speed conditions as well. The efficiency values predicted by using these published μ formulae would be much lower than the actual mechanical efficiency values. Therefore, it can be concluded here that these formulae should not be used for gear efficiency studies and the results of previous efficiency models that employed these formulae [34-37, 40] should be taken cautiously. On the other hand, EHL model predictions agree well with the measured friction coefficient data for typical ranges of speed, load, and sliding ratio. The μ values predicted by the EHL model and the measured values represented by the fitted formula are compared in Fig. 5 for $P_h = 1.0$ GPa and $V_e = 10$ and 20 m/s.

Based on this comparison, the EHL-based model can be considered valid. This is a positive outcome since the EHL model is physics-based requiring no empirical parameters. However, it presents a major difficulty especially when used in a gear efficiency model. Each EHL analysis takes several minutes of computations (more than 2 minutes of CPU time on a 3.0 GHz PC) and a complete gear efficiency analysis might require a few hundred EHL analyses. Therefore, this approach is not practical for real-life engineering applications requiring many parameter studies. In order to overcome this disadvantage, a design of experiment (DOE) of the EHL model is performed. Results from DOE were processed by multiple linear regression analysis to obtain a new μ formula based on the EHL approach to be used in the gear efficiency models, eliminating the difficulties of this approach in terms of the computational demand. The new formula has the form

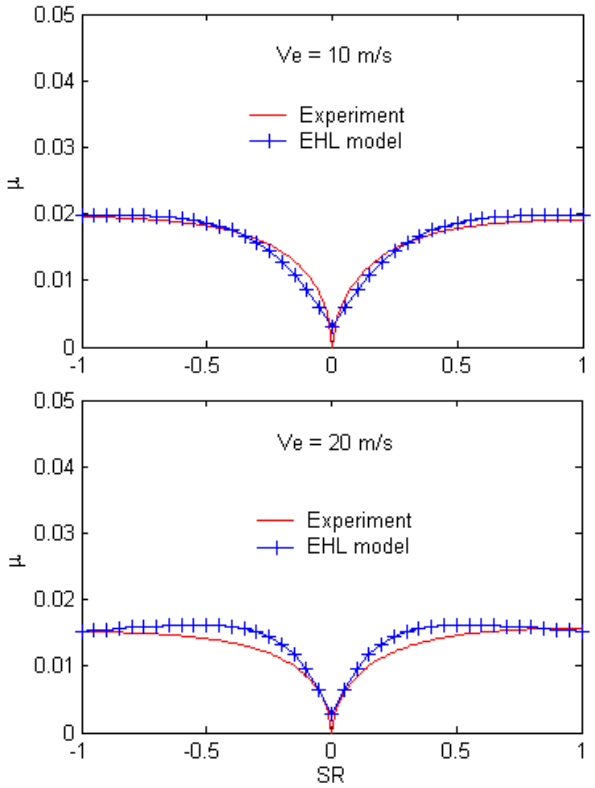

Figure 5. Comparison of EHL model predictions and the measured data at $P_h = 1$ GPa and various V_e values.

$$\mu = e^{f(SR,P_h,\nu_0,S)} P_h^{b_2} |SR|^{b_3} V_e^{b_6} \nu_0^{b_7} R^{b_8} \quad (31)$$

where

$$f(SR,P_h,\nu_0,S) = b_1 + b_4 |SR| P_h \log_{10}(\nu_0) + b_5 e^{-|SR|P_h \log_{10}(\nu_0)} + b_9 e^S$$

Constants b_1 to b_9 vary based on type of lubricant used. This formula includes all the key features of a gear contact, namely SR, V_e, P_h, S, R, and ν_0. It can be directly used to calculate μ instead of running extremely time-consuming EHL analyses in real time, while still maintaining acceptable accuracy. It also avoids numerical issues associated with any EHL model. The same equation was used earlier in a spur gear mechanical efficiency prediction model that was validated through high-speed spur gear efficiency measurements [77].

3 Results and Discussions

With all necessary parameters at each contact point calculated by using the formulations and the contact model presented in previous sections, instantaneous efficiency of a hypoid gear pair can be calculated by applying the methodology defined in Fig. 1. A face-hobbed hypoid gear pair borrowed from an automotive application will be used here as an example system to demonstrate the hypoid gear efficiency methodology. The main gear blank dimensions of this example system are listed in Table 2. The pinion member is generated and the ring gear is non-generated. A typical gear oil 75W90 is used as the lubricant whose properties are listed in Table 3.

Table 2 Example hypoid gear pair

Parameters	Pinion	Gear
Teeth number	12	41
Hand of spiral	Left	Right
Spiral angle (*deg*)	49.97	24.07
Outer cone distance (*mm*)	103.5	127.7
Face width (*mm*)	41.9	34.2
Face angle (*deg*)	28.6	58.7
Pitch angle (*deg*)	28.6	58.7
Front/Back angles (*deg*)	28.6	58.7
Pinion offset (*mm*)	44	
Shaft angle (*deg*)	90	
Material density (kg/m^3)	7800	
Specific heat (*J/kg K*)	500	
Thermal conductivity (*W/m K*)	45	
Young's modulus (*Pa*)	2.07×10^{11}	
Poisson's ratio	0.3	

Table 3 Lubricant parameters

Inlet temperature (*K*)	333
Viscosity (*Pa s*)	0.036
Density (*kg/m3*)	815
Pressure viscosity coefficient (*1/Pa*)	1.344×10^{-8}
Temperature viscosity coefficient	0.0217
Thermal conductivity (*W/m K*)	0.132
Coefficient of thermal expansion	6.5×10^{-4}
Specific heat (*J/kg K*)	2000

Figure 6 illustrates the contact pressures distribution at all the contact zones on the hypoid ring gear in contact at a given mesh position. As discussed earlier, contact pressures, radii of curvatures, sliding velocities, and sum of rolling velocities are four of the key geometry-related parameters used in the friction model. The distributions of these parameters along the contact lines at the same mesh angle $\phi = \phi_1$ are shown in Fig. 7. It is clear from this figure that all four key parameters vary significantly along the contact lines.

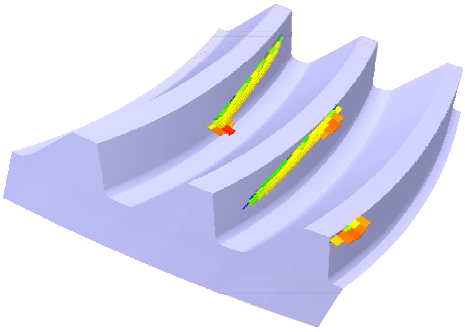

Figure 6. Contact pressure distribution prediction of CALYX at a given mesh position ϕ_1.

(a) $P_{\max} = 4.4$ GPa, $P_{\min} = 0.036$ GPa

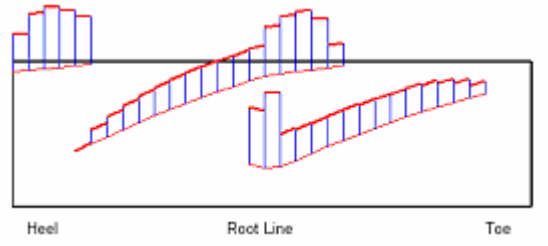

(b) $R_{\max} = 76$ mm, $R_{\min} = 2$ mm

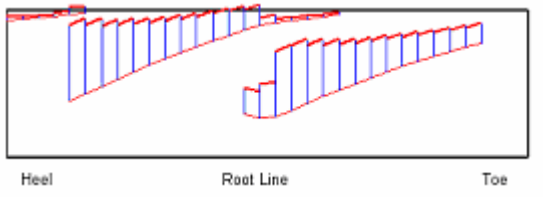

(c) $V_{s,\max} = 1.8$ m/s, $V_{s,\min} = 0.02$ m/s

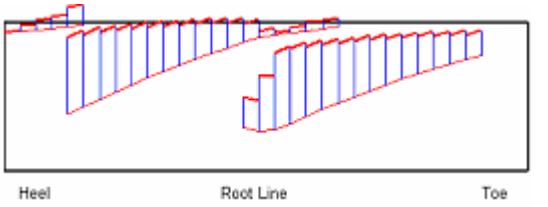

(d) $V_{r,\max} = 8.0$ m/s, $V_{r,\min} = 0.6$ m/s

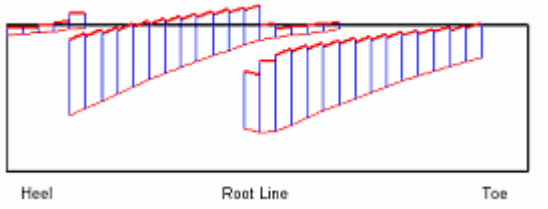

Figure 7. Distribution of (a) contact pressure, (b) combined radii of curvature, (c) sliding velocity, and (d) sum of rolling velocities along the normal of the instant line of contact at mesh position ϕ_1. $S = 0.1\ \mu m$, $L_{in} = 1{,}600\ Nm$, $N_p = 1{,}000\ rpm$, and $T_{oil} = 60^{\circ}C$.

(a) EHL-based μ formula

$\mu_{\max} = 0.0857$, $\mu_{\min} = 0.0063$

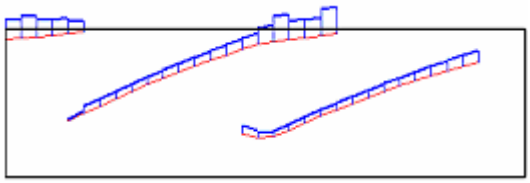

(b) Actual EHL analysis

$\mu_{\max} = 0.1023$, $\mu_{\min} = 0.0156$

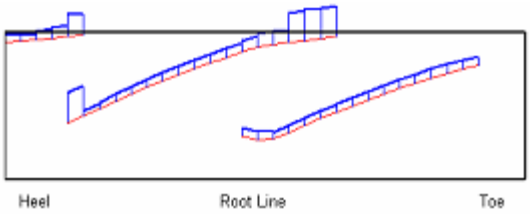

Figure 8. Distribution of $\mu(z,\theta,\phi_1)$ at every mesh grid of principal contact points predicted by using (a) the EHL-based μ formula, and (b) actual EHL analysis. $S = 0.1\ \mu m$, $L_{in} = 1{,}600\ Nm$, $N_p = 1{,}000\ rpm$, and $T_{oil} = 60^{\circ}C$.

The values of $\mu(z,\theta,\phi_1)$ at each of the principal contact points along the instantaneous lines of contact are calculated by using the new formula in Eq. (31) as well as the actual EHL model are shown in Fig. 8 for $S = 0.1\ \mu m$, $L_{in} = 1{,}600\ Nm$, $N_p = 1{,}000\ rpm$, and $T_{oil} = 60^{\circ}C$. For the EHL model prediction, a measured rough surface profile with $RMS = 0.1\ \mu m$ like the one shown in Fig. 9 is used. As shown in Fig. 8, the predicted μ values show certain amount of variations along the instantaneous lines of contact. The μ values become especially large when the contact occurs near the edge where contact pressures are large as shown in Fig. 7. The variations of μ predicted at each contact point, together with the variations of the contact pressures and the sliding and rolling velocities, result in the variations of the power losses at each of these locations.

Figure 10 shows the variation of the average value of the instantaneous coefficient of friction at every mesh angle, $\bar{\mu}(\phi_m) = Average[\mu(z,\theta,\phi_m)]$, and the corresponding instantaneous mechanical efficiency $\eta(\phi_m)$ of the gear pair. It is evident that the two EHL related models are in reasonably good agreement and give an average efficiency of about $\eta = 98$ percent for $S = 0.1\ \mu m$, $L_{in} = 1{,}600\ Nm$, $N_p = 1{,}000\ rpm$ and $T_{oil} = 60^{\circ}C$.

A parametric study on the mechanical efficiency of the example hypoid gear pair is performed next. Figure 11 shows the variation of $\bar{\eta}$ as a function of N_p for $L_{in} = 500$ and $1{,}000$, given $S = 0.4\ \mu m$ and $T_{oil} = 60^{\circ}C$. L_{in} has a negligible influence on $\bar{\eta}$

within this load range and curves for $L_{in} = 500$ and $1{,}000$ Nm are almost identical. However, $\bar{\eta}$ increases quite significantly with an increase in N_p. The mechanical efficiency values at $N_p = 500$ and $2{,}000$ rpm differ by nearly 2 percent, which is due to very small rolling velocities at low speed that cause the friction coefficient increase significantly.

The combined influence of the surface roughness parameter S and the oil inlet temperature T_{oil} is illustrated in Fig. 12 for $L_{in} = 1{,}600$ Nm and $N_p = 1{,}000$ rpm. Both T_{oil} and S have a significant influence on $\bar{\eta}$. For instance at $T_{oil} = 60^{\circ}C$, $\bar{\eta} = 98.3$ percent for a smooth surface while it is 96.3 percent for $S = 0.6$ μm. At the same roughness value of $S = 0.6$ μm, elevating lubricant temperature to $100^{\circ}C$ improves the efficiency from 96.3 percent to nearly 97.5 percent, partly due to the reduction in viscosity due to temperature increment [77,78].

Influence of hypoid gear assembly tolerances or errors, H, V, R, and β that are defined in Fig. 13 on $\bar{\eta}$ are shown in Fig. 14. In Fig. 15, H, V, and R are all varied from –0.5 *mm* to +0.5 *mm* and β is varied from –0.1 degree to +0.1 degree. From Fig. 14, it is found that shaft angle error β has almost no influence on $\bar{\eta}$, while influence of other three errors on $\bar{\eta}$ is very limited for the cases considered.

4 Conclusions

A model for the prediction of hypoid gears has been proposed and applied to a face-hobbed hypoid gear pair as a representative example. Formulations for the required surface velocities and radii of curvature have been presented. Influence of operating conditions, surface finish and lubricant temperature, as well as assembly errors on the efficiency of hypoid gears have also been quantified. While hypoid gear pair is defined by a very large number of parameters, extensive generic analyses were not possible to obtain information about the influence of each parameter on the mechanical efficiency of the hypoid gear pair, still several consistent trends were observed. The rotational speed, surface roughness amplitude, and lubricant temperature are all very influential on the mechanical efficiency of a hypoid gear pair. Meanwhile, the parameters such as load and assemble errors have a limited or no influence on hypoid efficiency.

Acknowledgement

Authors thank AGMA Foundation for sponsoring a portion of this work. Authors also thank Advanced Numerical Solutions, Inc. for making the hypoid gear analysis package CALYX available.

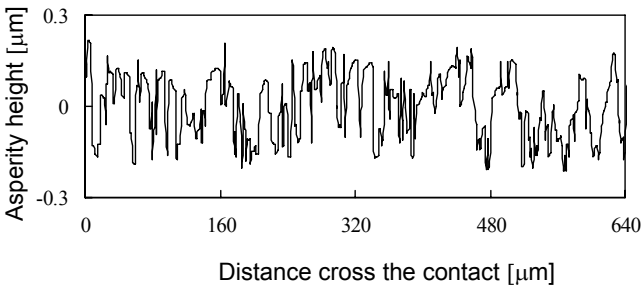

Figure 9. A measured surface roughness profile used in the EHL analysis.

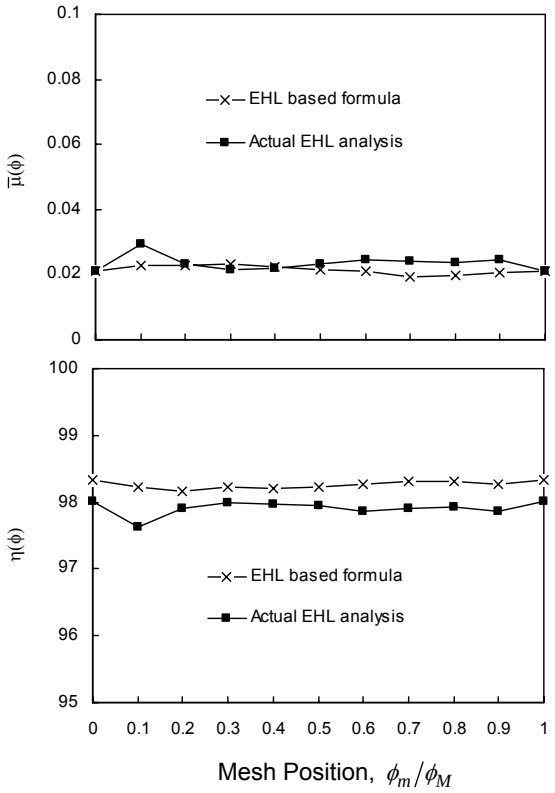

Figure 10. $\bar{\mu}(\phi)$ and $\eta(\phi)$ predicted by using the friction coefficient formulae developed in this study and the EHL model. $S = 0.1\ \mu m$, $L_{in} = 1{,}600\ Nm$, $N_p = 1{,}000\ rpm$, and $T_{oil} = 60^{\circ}C$.

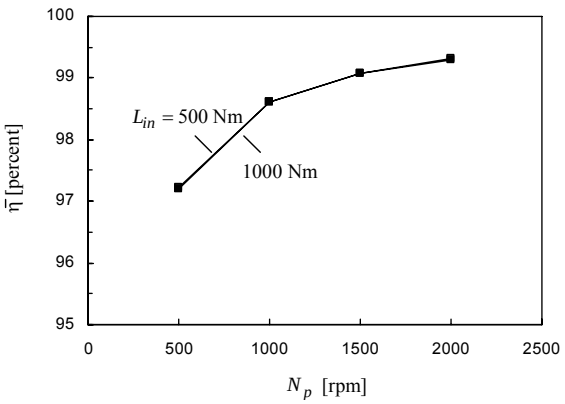

Figure 11. Influence of L_{in} and N_p on $\bar{\eta}$; $S = 0.4\ \mu m$ and $T_{oil} = 60^{\circ}C$.

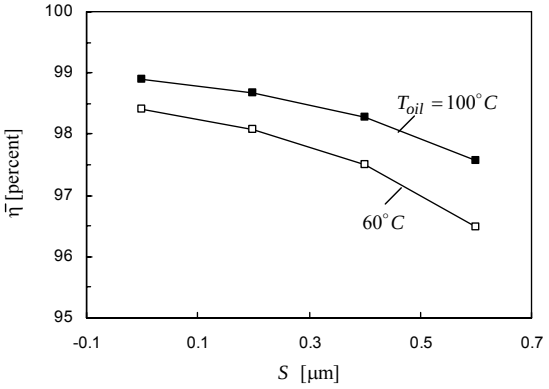

Figure 12. Influence of S and T_{oil} on $\bar{\eta}$; $L_{in} = 1,600\ Nm$ and $N_p = 1,000\ rpm$.

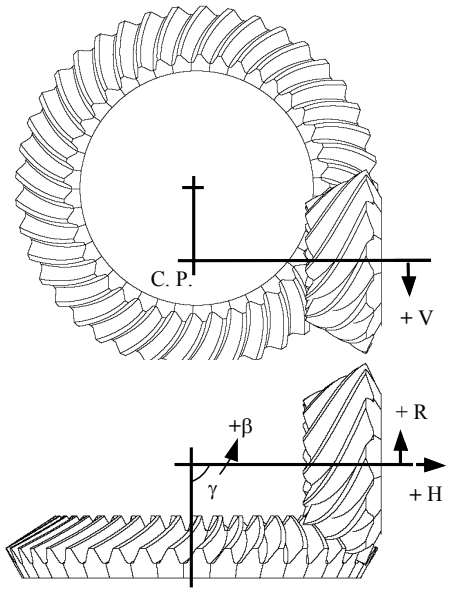

Figure 13. Example hypoid gear pair geometry and illustration of errors, V: pinion movement along offset, H: pinion axial movement, R: pinion movement along gear axis, β: shaft angle error.

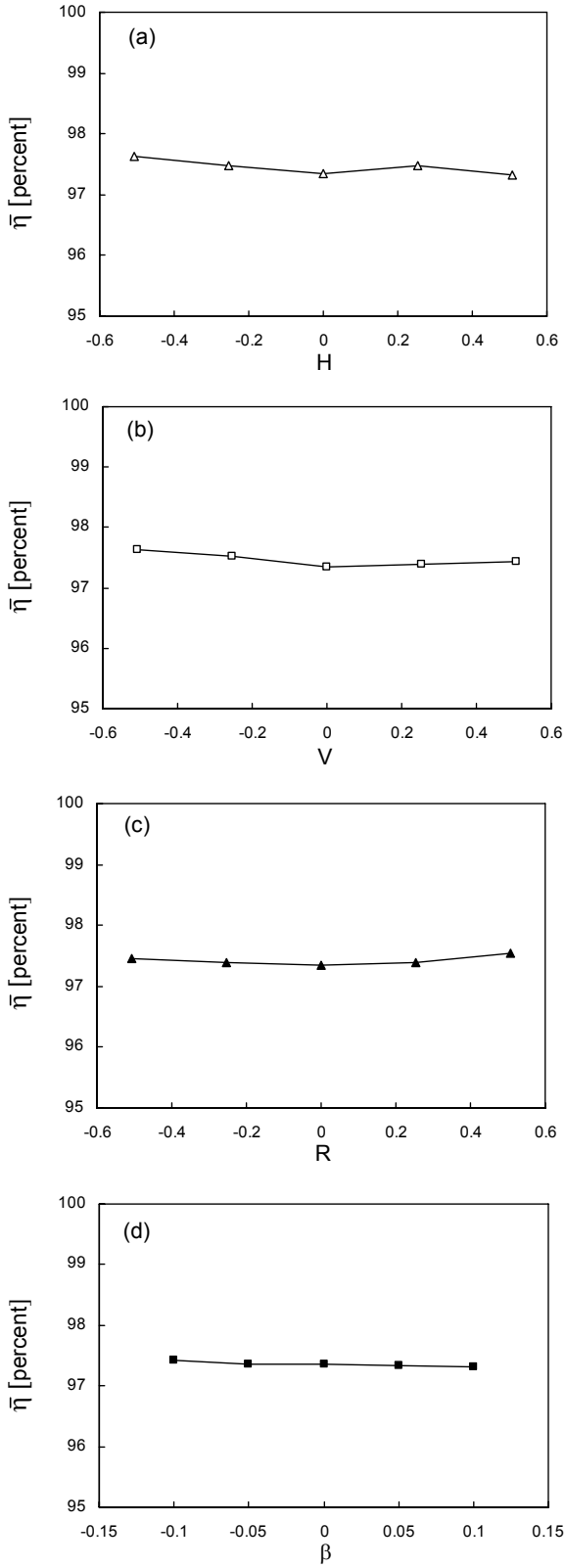

Figure 14. Influence of errors (a) H, (b) V, (c) R, and (d) β on $\bar{\eta}$. $S = 0.4\ \mu m$, $L_{in} = 1,600\ Nm$, $N_p = 1,000\ rpm$, and $T_{oil} = 60^{\circ}C$.

References

[1] Reuleaux, F., “Friction in Tooth Gearing”, Transactions of the ASME, Vol. VIII, pp. 45-85, 1886.

[2] Vaishya, M., Houser, D. R., “Modeling and Analysis of Sliding Friction in Gear Dynamics”, DETC’00, Baltimore, Maryland, 2000.

[3] Hochmann, D., Houser, D. R., “Friction Forces as a Dynamic Excitation Source in Involute Spur and Helical Gearing”, DETC’00/PTG, Baltimore, Maryland, 2000.

[4] Hamrock, B. J., “Fundamentals of Fluid Film Lubrication”, NASA reference publication, 1991.

[5] Martin, K. F., “A Review of Friction Predictions in Gear Teeth”, Wear 49, pp. 201-238, 1978.

[6] Yada, T., “Review of Gear Efficiency Equation and Force Treatment”, JSME International Journal, Series C, Vol. 40, pp. 1- 8, 1997.

[7] Li, Y., Seireg, A. A., “Predicting The Coefficient of Friction in Sliding-Rolling Contacts”, Tribology Conference, K18.

[8] Naruse, C., Haizuka, S., Nemoto, R., and Suganuma, T., “Studies on Limiting Load for Scoring and Frictional Loss of Hypoid Gears of Klingelnberg Type”, Bulletin of JSME, Vol. 27, No. 231, pp. 2053-2060, 1984.

[9] Naruse, C., Haizuka, S., Nemoto, R., and Kurokawa, K., “Studies on Frictional Loss, Temperature Rise and Limiting Load for Scoring of Spur Gear”, Bulletin of JSME, Vol. 29, No. 248, pp. 600-608, February, 1986.

[10] Naruse, C., Haizuka, S., Nemoto, R., and Umezu, T., “Limiting Loads for Scoring and Frictinal Loss of Hypoid Gear”, Bulletin of JSME, Vol. 29, No. 253, pp. 2271-2280, July, 1986.

[11] Naruse, C., Haizuka, S., Nemoto, R., and Takahashi, H., “Influences of Tooth Profile on Frictional Loss and Scoring Strength in The Case of Spur Gears”, MPT’91 JSME Int’l Conference on Motion and Power Transmissions, Hiroshima, Japan, 1991.

[12] Mizutani, H. and Isikawa, Y., “Power Loss of Long Addendum Spur Gears”, VDI Berichte NR. 1230, pp. 83-95, 1996.

[13] Hori, K., Hayashi, I., Iwatsuki, N., “Determination of the Tooth Surface Friction Coefficient of a Pair of Mating Gears Based on the Distribution along the Tooth Profile Precisely Measured with the Gravity Pendulum Method”, Proceedings of DETC’00/PTG-14371, Baltimore, Maryland, September10-13, 2000.

[14] Yoshino, H., Ohshima, F., “Effects of Tooth Profiles and Addendum Modification on Efficiency of Cylindrical Worm Gears”, Proceedings of DETC’00/ PTG-14399, Baltimore, Maryland, Sept. 10-13, 2000.

[15] Yada, T., “The Measurement of Gear Mesh Friction Losses”, ASME 72-PTG-35, October 8-12, 1972.

[16] Changenet, C., Pasquier, M., “Power Losses and Heat Exchange in Reduction Gears: Numerical and Experimental Results”, VDI Berichte NR.1665, pp.603-613, 2002.

[17] Ikejo, K., Nagamura, K., “Power Loss of Spur Gear Drive Lubricated with Traction Oil”, DETC’03/PTG, Chicago, Illinois, 2003.

[18] Misharin, Y. A., “Influence of The Friction Condition on The Magnitude of The Friction Coefficient in The Case of Rollers with Sliding”, Proc. Int. Conf. On Gearing, 1958, Inst. Mech. Eng., London, pp. 159-164, 1958.

[19] Benedict, G. H. and Kelly, B. W., “Instantaneous Coefficients of Gear Tooth Friction”, Transactions of ASLE, ASLE Lubrication Conference, pp.57-70, October, 1960.

[20] O’Donoghue, J. P., Cameron, A., “Friction and Temperature in Rolling Sliding Contacts”, ASLE Transactions 9, pp. 186-194, 1966.

[21] Drozdov, Y. N. and Gavrikov, Y. A., “Friction and Scoring Under The Conditions of Simultaneous Rolling and Sliding of Bodies”, Wear, pp. 291-302, 1967.

[22] Plint, M.A., Mech, F.I.E., “Traction in Elastohydrodynamic Contacts”, Proc. Instn. Mech. Engrs. Vol. 182, Pt. 1, No. 14, 1967-68.

[23] Kelley, B. W. and Lemanski, A. J., “Lubrication of Involute Gearing”, Proc. Instn. Mech. Engrs, Vol. 182, pp.173-184, 1967-1968.

[24] Ku, P. M., Staph, H. E. and Carper, H. J., “Frictional and Thermal Behaviors of Sliding-rolling Concentrated Contacts”, Journal of Lubrication Technology, Vol.100, pp. 121-128, 1978.

[25] Naruse, C., Haizuka, S., “Limiting Loads for Scoring and Coefficient of Frictin on a Disk-Machine (Effects of Lubricating Oil, Specific Sliding and Sliding Velocity, in the Case of Steel/Steel)”, Bulletin of JSME, Vol. 21, No. 158, pp. 1311-1317, 1978.

[26] Mihallidis, A., Salpistis, C., Drivakos, N., Panagiotidis, K., “Friction Behavior of FVA Reference Mineral Oils Obtained by a Newly Designed Two-Disk Test Rig”, International Conference: Power Transmissions’03.

[27] Hirano, F., Ueno, T, Asanabe, S., “Effect of Angle Between Direction of Sliding and Line of Contact on Friction and Wear of a Roller”, Lubrication Engineering, pp. 57-64, 1964.

[28] Tan, J., Yamada, T., Hattori, N., “Effects of Sliding/Rolling Contact on Worm Gear Lubrication”, The JSME international Conference on Motion and Power Transmissions, Hiroshima, Japan. pp.11231127, 1991.

[29] Hohn, B.-R., Winter, H., Michaelis, K., Steingrover, K., “Friction and Efficiency of Worm Gears”, 3rd World Congress on Gearing and Power Transmissions, Paris, France. pp.235-245, 1992.

[30] Bercsey, T., Horak, P., “Modeling of the Contact and Tribological Relations of Spatial Gear Pairs”, VDI Berichte NR.1665, pp.91-105, 2002.

[31] Denny, C. M., “Mesh Friction in Gearing”, AGMA Fall Technical Meeting, 98FTM2, 1998.

[32] Pedrero, J. I., “Determination of The Efficiency of Cylindrical Gear Sets”, 4th World Congress on Gearing and Power Transmission, Paris, France, March, 1999.

[33] Michlin, Y., Myunster,V., “Determination of Power Losses in Gear Transmissions with Rolling and Sliding Friction Incorporated”, Mechanism and Machine Theory, Vol. 37, pp. 167, 2002.

[34] Heingartner, P., Mba, D., “Determining Power Losses in The Helical Gear Mesh; Case Study”, DETC’3, Chicago, Illinois, 2003.

[35] Anderson, N. E., Loewenthal, S. H., “Efficiency of Nonstandard and High Contact Ratio Involute Spur Gears, ” Journal of Mechanisms, Transmissions, and Automation in Design, Vol. 108, pp. 119-126, 1986.

[36] Anderson, N. E., Loewenthal, S. H., “Design of Spur Gears for Improved Efficiency”, ASME, JMD, Vol. 104, pp. 767-774, 1982.

[37] Anderson, N. E., Loewenthal, S. H., “Effect of Geometry and Operating Conditions on Spur Gear System Power Loss”, Journal of Mechanical Design, Vol. 103, pp. 151-159, 1981.

[38] Barnes, J. P., “Non-Dimensional Characterization of Gear Geometry, Mesh Loss and Windage”, 97FTM11, November, 1997.

[39] Hohn, B. R., Steingrover, K., “Local Coefficients of Friction in Worm Gear Contacts”, 98FTM10, October, 1998.

[40] Vaishya, M., Houser, D. R., “Modeling and Measurement of Sliding Friction for Gear Analysis”, 99FTMS1, October 1999.

[41] ISO TC 60, DTR 13989

[42] Dudley, D. W., “Characteristics of regimes of Gear Lubrication”, Int’l Symposium on Gearing and Power Transmissions, Tokyo, Japan, 1981.

[43] Snidle, R. W., Evans, H. P., “Elastohydrodynamics of Gears”, Elastohydrodynamics ’96/Dowson et al. (Editors), pp.271-280, 1997.

[44] Crook, A. W., “A Theoretical Discussion of Friction and The Temperatures in The Oil Film”, Phil. Trans. Roy. Soc. (London), Ser. A, Vol. 254, pp. 237-258, 1961.

[45] Dyson, A., “Frictional Traction and Lubricant Rheology in Elastohydrodynamic Lubrication”, Philosophical Transactions of the Royal Society of London, Series A, 266, pp.1-33, 1970.
[46] Trachman, E. G., “A Simplified Technique for Predicting Traction in Elastohydrodynamic Contacts”, ASLE Transactions, Vol.21, No.1, pp.53-69, 1977.
[47] Dowson, D., Higginson, G. R., “A Theory of Involute Gear Lubrication”, Proceeding of a Symposium Organized by the Mechanical Tests of Lubricants Panel of the Institute, Institute of Petroleum, Gear Lubrication, Elsevier, London, pp. 8-15, 1964.
[48] Martin, K. F., “The Efficiency of Involute Spur Gears”, Journal of Mechanical Design. Vol. 103, pp. 160-169, 1981.
[49] Adkins, R. W., Radzimovsky, E. I., “Lubrication Phenomena in Spur Gears: Capacity, Film Thickness Variation, and Efficiency”, Journal of Basic Engineering, pp. 1-9, 1964.
[50] Simon, V., “Load Capacity and Efficiency of Spur Gears in Regard to Thermo-End Lubrication”, International Symposium on Gearing and Power Transmissions, Tokyo, Japan, 1981.
[51] Larsson, R., “Transient Non-Newtonian Elastohydrodynamic Lubrication Analysis of an Involute Spur Gears”, Wear, Vol. 207, pp.67-73, 1997.
[52] Wang, Y., Li, H., Tong, J., Yang, P., “Transient Thermalelastohydrodynamic Lubrication Analysis of an Involute Spur Gear”, Tribology International, Vol. 37, pp. 773-782, 2004.
[53] Wu, S., Cheng, H., S., “A Friction Model of Partial-EHL Contacts and its Application to Power Loss in Spur Gears”, Tribology Transactions, Vol. 34, No. 3, pp.398-407, 1991.
[54] Mihalidis, A., Bakolas, V., Panagiotidis, K., Drivakos, N., “Predition of The Friction Coefficient of Spur Gear Pairs”, VDI-Berichte, NR. 1665, pp. 705-719, 2002.
[55] Akin, L. S., “EHD Lubricant Film Thickness Formulae for Power Transmission Gears”, ASME Journal of Lubrication Technology, pp.426-431, 1974.
[56] Wellauer, E. J. and Holloway, S. H., “Application of EHD Oil Film Theory to Industrial Gear Drives”, ASME Journal of Engineering for Industry, pp.626-634, 1976.
[57] Chittenden, R. J., Dowson, D., Dunn, J. F., and Taylor, C. M., “A Theoretical Analysis of The Isothermal Elastohydrodynamic Lubricant of Concentrated Contacts”, Proc. R. Soc. Lond. A 397, pp.271-294, 1985.
[58] Simon, V., “Thermo-EHD Analysis of Lubrication of Helical Gears”, Journal of Mechanical Design, Vol.110, pp.330-336, 1988.
[59] Buckingham, E., “Efficiencies of Gears”, Analytical Mechanics of Gears, Dover, New York, pp. 395-425, 1963.
[60] Coleman, W., “A Scoring Formula for Bevel and Hypoid Gear teeth”, Transaction of the ASME, Journal of Lubrication Technology, Ser. F87-2, pp.114-126, 1967.
[61] Coleman, W., “Computing Efficiency for Bevel and Hypoid Gears”, Machine Design, pp.64-65, 1975.
[62] Simon, V., “Elastohydrodynamic Lubrication of Hypoid Gears”, Journal of Mechanical Design, Vol. 103, pp.195-203, 1981.
[63] Jia, Y., Guo, X., Chen, C., Shao, J., “Multilevel Solution of Elastohydrodynamically Lubricated Hypoid Gears”, International Gearing Conference, University of Newcastle upon Tyne, UK. pp.329-334, 1994.
[64] Shipley, E. E., “Loaded Gears in Action”, Gear Handbook, First Edition, Dudley, D. W., McGraw-Hill, 1962.
[65] Dawson, P. H., “Windage Losses in Larger, High Speed Gears”, Proc. Instn. Mech. Engrs, 198A(1), pp.51-59, 1984.
[66] Dawson, P. H., “High-speed Gear Windage”, GEC Review, Vol. 4, No. 3pp.164-167, 1988.
[67] Luke, P. and Olver, A, “A Study of Churning Losses in Dip-lubricated Spur Gears”, Proc. Instn. Mech. Engrs, Vol. 213, Part G, pp.337-346, 1999.
[68] Khonsari, M. M. and Booser E. R., “Applied Tribology, Bearing design and Lubrication”, John Wiley & Sons, 2001.
[69] Dian, Y., Ville, F., Velex, P., and Changenet, C., “Windage Losses in High Speed Gears Preliminary Experimental and Theoretical Results”, Journal of Mechanical Design, Vol. 126, pp.903-908, 2004.
[70] Xu, H., Kahraman, A., “A Frictional Efficiency Loss Model for Helical Gears”, DETC2005-85243, Proceedings of IDETC/CIE 2005, ASME 2005 International Design Engineering Technical Conferences and Computers and Information in Engineering Conference, Long Beach, CA, Sept 24-28, 2005.
[71] Vijayakar, S., CALYX manual, Advanced Nemerical Solutions Inc., Columbus, Ohio, 2000.
[72] Vijayakar, S., “A Combined Surface Integral and Finite Element Solution for a Three-Dimensional Contact Problem”, Internaltional Journal for Numerical Methods in engineering, Vol. 31, pp525-545, 1991.
[73] Struik, D. J., “Lectures on Classical Differential Geometry”, Cambridge, Mass., Addison-Wesley Press, 1950.
[74] Litvin, F. L., “Gear Geometry and Applied Theory”, Prentice Hall, Englewood Cliffs, New Jersey, 1994.
[75] Cioc, C., Cioc, S., Moraru, L., Kahraman, A., and Keith, T., “A deterministic Elastohydrodynamic Lubrication Model of High-speed Rotorcraft Transmission Components”, Tribology Transactions, Vol. 45, pp. 556-562, 2002.
[76] Dowson, D., Higginson, G. R., “Elasto-hydrodynamic Lubrication”, SI Edition, Pergamon Press, Oxford, England, 1977.
[77] Xu, H., “Development of a Generalized Mechanical Efficiency Prediction Methodology for Gear Pairs”, Ph.D. Dissertation, The Ohio State University, Columbus, Ohio, 2005.
[78] Johnson, K. L., Cameron, R., “Shear Behavior of Elastohydrodynamic Oil Films at High Rolling Contact Pressures”, Proc. Instn. Mech. Engrs, Vol. 182, Pt. 1, No. 14, pp. 307-319, 1967-68.